ACS APPLIED MATERIALS & INTERFACES

Research Article

www.acsami.org

Influence of the Hole Transporting Layer on the Thermal Stability of Inverted Organic Photovoltaics Using Accelerated-Heat Lifetime Protocols

Felix Hermerschmidt,[†] Achilleas Savva,[†] Efthymios Georgiou,[†] Sachetan M. Tuladhar,[‡] James R. Durrant,[§] Iain McCulloch,[§] Donal D. C. Bradley,[∥] Christoph J. Brabec,[⊥] Jenny Nelson,[‡] and Stelios A. Choulis*[,†]

[†]Molecular Electronics and Photonics Research Unit, Department of Mechanical Engineering and Materials Science and Engineering, Cyprus University of Technology, 3041 Limassol, Cyprus

[‡]Department of Physics and [§]Department of Chemistry, Imperial College London, London SW7 2AZ, U.K.

[∥]Departments of Engineering Science and Physics, Division of Mathematical, Physical and Life Sciences, University of Oxford, Oxford OX1 3PD, U.K.

[⊥]Institute for Materials in Electronics and Energy Technology, Friedrich-Alexander University Erlangen-Nuremberg, 91054 Erlangen, Germany

ABSTRACT: High power conversion efficiency (PCE) inverted organic photovoltaics (OPVs) usually use thermally evaporated MoO_3 as a hole transporting layer (HTL). Despite the high PCE values reported, stability investigations are still limited and the exact degradation mechanisms of inverted OPVs using thermally evaporated MoO_3 HTL remain unclear under different environmental stress factors. In this study, we monitor the accelerated lifetime performance under the ISOS-D-2 protocol (heat conditions 65 °C) of nonencapsulated inverted OPVs based on the thiophene-based active layer materials poly(3-hexylthiophene) (P3HT), poly[[4,8-bis[(2-ethylhexyl)oxy]benzo[1,2-*b*:4,5-*b*′]dithiophene-2,6-diyl][3-fluoro-2-[(2-ethylhexyl)carbonyl]thieno[3,4-*b*]thiophenediyl]] (PTB7), and thieno[3,2-*b*]thiophene-diketopyrrolopyrrole (DPPTTT) blended with [6,6]-phenyl C_{71}-butyric acid methyl ester (PC[70]BM). The presented investigation of degradation mechanisms focus on optimized P3HT:PC[70]BM-based inverted OPVs. Specifically, we present a systematic study on the thermal stability of inverted P3HT:PC[70]BM OPVs using solution-processed poly(3,4-ethylenedioxythiophene):polystyrene sulfonate (PEDOT:PSS) and evaporated MoO_3 HTL. Using a series of measurements and reverse engineering methods, we report that the P3HT:PC[70]BM/MoO_3 interface is the main origin of failure of the P3HT:PC[70]BM-based inverted OPVs under intense heat conditions, a trend that is also observed for the other two thiophene-based polymers used in this study.

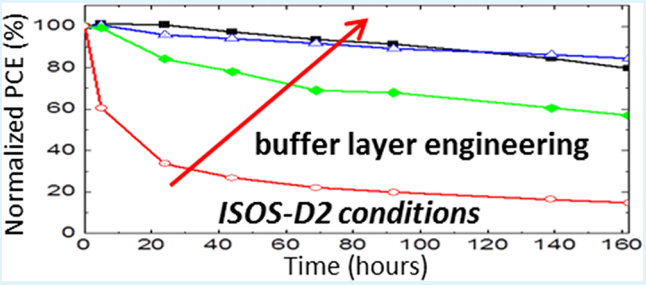

KEYWORDS: *organic photovoltaics, inverted structure, thermal stability, ISOS-D-2 protocol, lifetime, degradation mechanism, hole-transporting layer, buffer layer engineering*

1. INTRODUCTION

Organic photovoltaics (OPVs) have attracted great scientific interest during the past decade because of their ease of manufacture with printable techniques and their potential to become flexible, lightweight, and low-cost energy sources.[1,2] High power conversion efficiencies (PCEs) and prolonged lifetimes are essential for OPV commercialization. Exciting PCEs of 10% have been demonstrated,[3] but long stabilities of OPVs are the next barrier that needs to be overcome. Understanding the degradation mechanisms that influence the stability of different device configurations under various environmental stress factors is still a challenging task.

In the inverted structure,[4,5] the use of an air-stable metal such as silver results in enhanced lifetime compared with normal structured OPVs, which are limited in stability mainly because of the oxidation of the metals such as calcium or aluminum.[6] Poly(3,4-ethylenedioxythiophene):polystyrene sulfonate (PEDOT:PSS) is the most common material used as the hole-transporting layer (HTL) in both architectures. It is known that because of its hygroscopic nature, ingress of moisture and oxygen from the edges into the device can cause degradation.[7,8]

Furthermore, heat is one of the environmental factors found to significantly affect the long-term stability of OPVs. Heat stability studies at the operating temperature performed by

Received: January 24, 2017
Accepted: March 30, 2017
Published: March 30, 2017

DOI: 10.1021/acsami.7b01183
ACS Appl. Mater. Interfaces 2017, 9, 14136−14144

Sachs-Quintana et al. on normal structured OPVs show that a thin polymer layer forms at the back (metal) contact, which creates an electron barrier between the active layer and the cathode.[9] This is related to the interface between the back contact and the bulk heterojunction and is shown to be the first step in thermal degradation in organic solar cells with normal architecture and especially while using low glass-transition temperature-conjugated polymers. However, in inverted OPVs, this barrier formation is favorable as it helps hole selectivity. This feature has been claimed to be an additional advantage of inverted OPVs.[9] Thus, the inverted structure is preferable concerning product development targets as it can allow more design flexibility and prolonged lifetime.

However, despite its prolonged lifetime, the top electrode (the anode) of the inverted OPVs has been identified as one of the most vulnerable parts of the device under various environmental stress factors. Several studies were performed, which reveal the crucial influence of the interface between the active layer and HTL on the lifetime performance of the inverted OPVs.[10−13] Inverted OPVs with PEDOT:PSS treated with different wetting agents present different lifetime behaviors under accelerated humidity conditions, thereby showing the crucial influence of processing and HTL/active layer interface formation.[14] Furthermore, Norrman et al. have suggested that PEDOT:PSS is the main factor of degradation of inverted OPVs under ambient conditions. They have demonstrated that the phase separation of PEDOT:PSS into PEDOT-rich and PSS-rich regions and the active layer/PEDOT:PSS interface are the main sources of failure of the long-term lifetime of inverted OPVs.[15]

Therefore, substitution of the moisture-sensitive PEDOT:PSS in inverted OPVs with metal oxide HTLs such as MoO_3, V_2O_5, and WO_3 could be beneficial in some cases concerning the stability of inverted OPVs. However, the use of solution-processed metal oxides as HTLs in inverted OPVs is still challenging because major processing issues have to be addressed. Recent work has shown that solution-processed MoO_3 can be used to produce normal structure and inverted OPVs that are efficient and stable when used as the sole HTL[16,17] as well as when inserted in addition to PEDOT:PSS.[18] Mixing solution-based MoO_3 with PEDOT:PSS has also yielded efficient inverted solar cells.[19] However, evaporated metal oxides are still more widely used as HTLs in inverted OPVs, leading to high PCEs with optimum hole selectivity.

Evaporated MoO_3 is a promising material as an HTL in inverted OPVs in terms of efficiency because of the favorable energy-level alignment between its work function measured at 6.9 eV[20] and the highest occupied molecular orbital of typical active layers in the range of −5.0 eV for polythiophene-based materials.[21] There are promising developments regarding the stability of inverted OPVs comparing MoO_3 and PEDOT:PSS HTLs in air;[17] however, lifetime studies under humidity comparing MoO_3 and PEDOT:PSS HTLs show that evaporated MoO_3 is also very sensitive to moisture and leads to inverted OPVs with limited lifetime.[22] The reason is that oxygen and humidity ingress can alter the conductivity and work function of MoO_3.[23,24] On the other hand, the hygroscopic PEDOT:PSS in this architecture can act as a getter and protect the active layer from water interactions.[25] Furthermore, MoO_3 may undergo a change in the oxidation state of the Mo(VI) metal center under exposure to heat or UV light, leading to changes in its work function and its optical response. Under heat conditions, MoO_3 releases oxygen, leading to lower Mo oxidation states and a shift in the work function of the oxide.[24,26]

In addition, Voroshazi et al. have shown that the reduction of MoO_3 can also occur under heat in dark conditions in inverted OPVs with MoO_3/Ag/Al top contact because of the chemical interactions between MoO_3 and Al atoms.[27] Another aspect of the degradation mechanism of inverted OPVs with the aforementioned top electrode was pointed out by Rösch et al. through different imaging techniques, whereby they attributed the failure to the migration of silver and diffusion into the MoO_3 layer, changing its work function.[28] Greenbank et al. also discuss diffusion into the active layer, and its resulting weakening is correlated to the decline (specifically J_{sc} reduction) in the device performance when used in conjunction with MoO_3 as the HTL.[29] However, a full understanding of the stability of MoO_3 HTL in inverted OPVs is still lacking because of the complexity of this material and the varying environmental stress factors that can influence the degradation cause of inverted OPVs with the MoO_3 HTL.

In this study, therefore, we aim to analyze the degradation mechanisms of nonencapsulated inverted OPVs using MoO_3 as the HTL, focusing on accelerated-heat lifetime conditions using the ISOS-D-2 protocol [dark, low relative humidity (RH), 65 °C]. As a first step, inverted OPVs using various polymer/fullerene active layers are investigated. Photocurrent mapping measurements provide degradation images at 65 °C at various points in time. Second, different electrode configurations are investigated for our reference poly(3-hexylthiophene):[6,6]-phenyl C_{71}-butyric acid methyl ester (P3HT:PC[70]BM) polymer/fullerene active layer. Using combinations of two interlayers—MoO_3 and PEDOT:PSS—at the top electrode of P3HT:PC[70]BM-based devices, the device degradation is attributed primarily to the interface between the active layer and MoO_3 and secondarily to that between MoO_3 and Ag. Third, alternative reverse engineering methods are used to enhance our assumption that the MoO_3/Ag interface significantly contributes to the degradation of devices under heat.

2. EXPERIMENTAL SECTION

Prepatterned glass−indium tin oxide (ITO) substrates (sheet resistance of 4 Ω/sq) were purchased from Psiotec Ltd. Zinc acetate dehydrate, 2-methoxyethanol, and ethanolamine were purchased from Sigma-Aldrich, P3HT was purchased from Rieke Metals, poly[[4,8-bis[(2-ethylhexyl)oxy]benzo[1,2-*b*:4,5-*b*′]dithiophene-2,6-diyl][3-fluoro-2-[(2-ethylhexyl)carbonyl]thieno[3,4-*b*]thiophenediyl]] (PTB7) was purchased from 1-Material, PC[70]BM was purchased from Solenne BV, PEDOT:PSS PH was purchased from H.C. Stark, MoO_3 powder was purchased from Sigma-Aldrich, and silver pellets were purchased from Kurt J. Lesker.

For the fabrication of inverted solar cells, ITO substrates were sonicated in acetone and subsequently in isopropanol for 10 min. The ZnO electron-transporting layer was prepared using a sol−gel process as described in detail elsewhere.[30] The ZnO precursor was doctor-bladed on the top of ITO substrates and annealed for 20 min at 140 °C under ambient conditions. After the annealing step, a 40 nm ZnO layer is formed as measured using a Veeco Dektak 150 profilometer. The photoactive layers, which are blends of 36 mg/mL in chlorobenzene P3HT:PC[70]BM (1:0.8 by weight), 15 mg/mL in *o*-DCB DPPTTT:PC[70]BM (1:2 by weight), and 25 mg/mL PTB7:PC[70]BM (1:1.5 by weight), were doctor-bladed on the top of ZnO, resulting in a layer thickness of ∼180, 100, and 90 nm, respectively, as measured with a profilometer.

DOI: 10.1021/acsami.7b01183
ACS Appl. Mater. Interfaces 2017, 9, 14136−14144

Table 1. Average Absolute Photovoltaic Parameter Values and Standard Deviation out of Eight Inverted OPVs in Each Case, Obtained before Initiating the Heat-Aging

inverted OPVs	V_{oc} (V)	J_{sc} (mA/cm^2)	FF (%)	PCE (%)
Active Layer/MoO_3/Ag				
P3HT:PC[70]BM	0.560 ± 0.009	11.17 ± 0.33	56.41 ± 1.69	3.54 ± 0.15
PTB7:PC[70]BM	0.678 ± 0.023	12.49 ± 0.55	46.75 ± 6.29	3.97 ± 0.67
DPPTTT:PC[70]BM	0.553 ± 0.010	11.22 ± 0.57	52.95 ± 3.73	3.32 ± 0.41
Active Layer/PEDOT:PSS:ZD/Ag				
P3HT:PC[70]BM	0.582 ± 0.007	9.26 ± 0.38	58.26 ± 2.56	3.16 ± 0.15
PTB7:PC[70]BM	0.691 ± 0.010	8.26 ± 0.68	50.28 ± 1.70	2.86 ± 0.31
DPPTTT:PC[70]BM	0.544 ± 0.008	8.07 ± 1.11	54.32 ± 1.42	2.53 ± 0.11

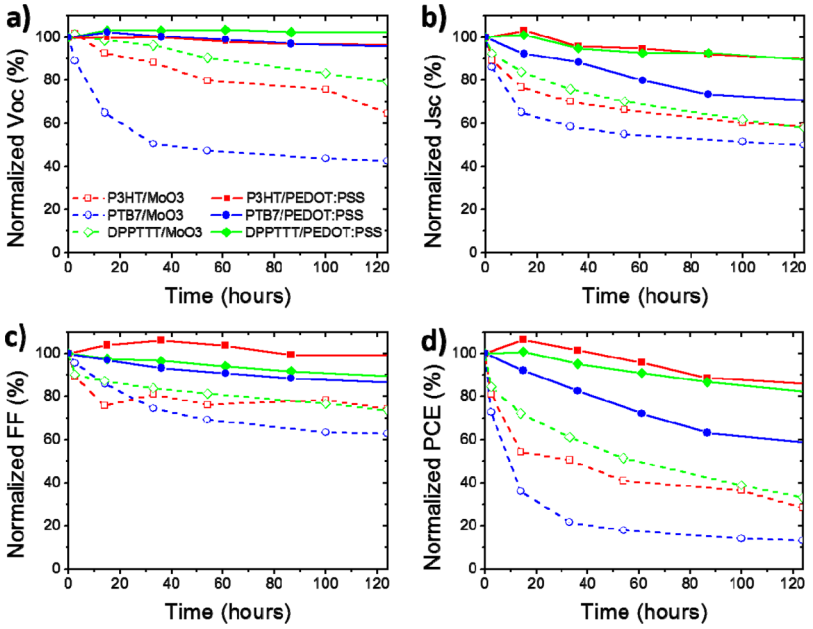

Figure 1. Degradation trends of the OPV parameters at 65 °C over time for nonencapsulated inverted OPVs with different active layers (red, P3HT:PC[70]BM; green, DPPTTT:PC[70]BM; and blue, PTB7:PC[70]BM) using either MoO_3 (dashed lines) or PEDOT:PSS (solid lines) as the HTLs, plotted as a function of (a) normalized V_{oc}, (b) normalized J_{sc}, (c) normalized fill factor (FF), and (d) normalized PCE.

All PEDOT:PSS-based devices were treated with two wetting agents (Zonyl and Dynol) as described in detail previously[14,31] (the resultant is referred to as PEDOT:PSS:ZD hereafter). The P3HT:PC[70]BM-based inverted OPVs were annealed inside of a glovebox at 140 °C for 20 min before thermal evaporation of a silver layer with a thickness of 100 nm, resulting in four solar cells, each with an active area of 9 mm^2. For the devices with the MoO_3 HTL, 10 nm of MoO_3 was evaporated before silver evaporation. For devices using MoO_3 and PEDOT:PSS:ZD as HTLs, MoO_3 was evaporated onto the active layer and PEDOT:PSS:ZD was doctor-bladed onto the MoO_3 layer followed by silver evaporation. These devices were annealed for another 2 min at 140 °C after the PEDOT:PSS:ZD deposition. For devices with a PEDOT:PSS:ZD/MoO_3/Ag top electrode, the procedure was the same as for PEDOT:PSS:ZD-based devices, except for an extra 10 nm MoO_3 layer evaporated on the top of the PEDOT:PSS:ZD layer.

The current density−voltage (J/V) characteristics were measured using a Keithley source measurement unit (SMU 2420). For illumination, a calibrated Newport Solar Simulator equipped with a Xe lamp was used, providing an AM 1.5G spectrum at 100 mW/cm^2 as measured using an Oriel 91150 V calibration cell equipped with a KG5 filter. Photocurrent measurements were recorded under a 405 nm laser excitation using a Botest PCT photocurrent system. Thermal aging of the devices was performed according to the ISOS-D-2 protocol;[32] namely, inverted OPVs under examination were placed in a dark chamber (Binder) at 65 °C with controlled ambient humidity of ∼45% and aged for several hours. Their J/V characteristics were measured at different stages of degradation. The devices were nonencapsulated, and the lifetime study was started 1 day after device fabrication.

3. RESULTS AND DISCUSSION

From our initial heat lifetime experiments comparing inverted OPVs comprised of ITO/ZnO/P3HT:PC[70]BM with a MoO_3/Ag versus PEDOT:PSS:ZD/Ag top electrode, we observed a dramatic drop in all photovoltaic parameters after just a few hours of aging of the inverted OPVs using MoO_3 as the HTL (data not shown).

3.1. Investigating the Degradation Mechanisms of Inverted OPVs under the ISOS-D-2 Protocol Using Different Polymer/Fullerene Blends and Top Electrode Configurations. To obtain a general picture about the heat degradation origins of inverted OPVs, three different polymer/fullerene blends were tested. The inverted OPVs with the following general configuration of ITO/ZnO/polymer:PC[70]BM/MoO_3/Ag or PEDOT:PSS:ZD/Ag were exposed to heat conditions based on the ISOS-D-2 protocol (T = 65 °C, dark, and constant ambient RH of ∼40%). P3HT:PC[70]BM (1:0.8),[30,33] PTB7:PC[70]BM (1:1.5),[34,35] and DPPTTT:PC[70]BM (1:4)[36,37] were used as the active layers. The polymer/fullerene ratios used were chosen from the best performing devices reported in the literature. The average

DOI: 10.1021/acsami.7b01183
ACS Appl. Mater. Interfaces 2017, 9, 14136−14144

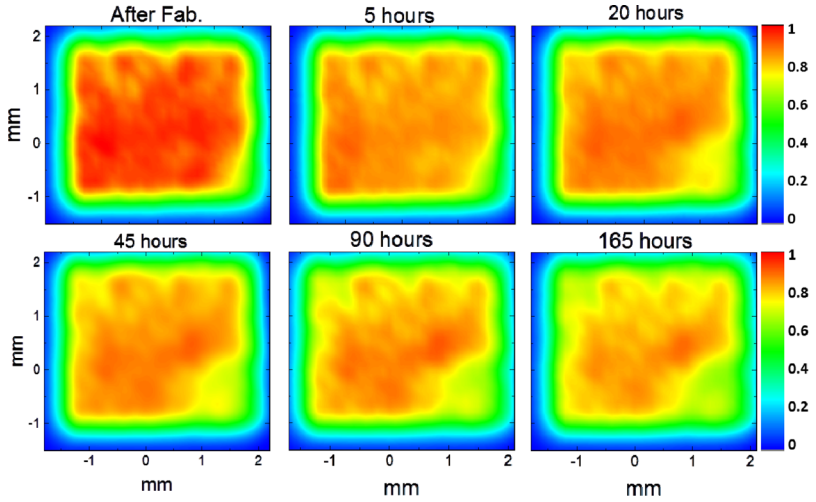

Figure 2. Normalized photocurrent mapping images of nonencapsulated inverted OPVs using MoO_3 as the HTL in P3HT:PC[70]BM-based solar cells, showing degradation at 65 °C over time of exposure.

absolute values of the photovoltaic parameters of the inverted OPVs under study were obtained just before starting the heat-aging and are summarized in Table 1.

It should be noted that although some of the device performance values presented in Table 1 may be below some literature values for the device structure, the purpose of this paper is not to produce best-performing "hero" devices. Thus, the relative performance values can still be used to obtain a general picture of the degradation behavior. Figure 1 shows the normalized photovoltaic parameters over time of exposure under heat conditions of all inverted OPVs under study.

As shown in Figure 1, photovoltaic parameters of all inverted OPVs with different polymer/fullerene blends using MoO_3/Ag top electrodes drop dramatically within the first few hours of exposure under accelerated-heat conditions. By contrast, the lifetime performance of the corresponding inverted OPVs using the PEDOT:PSS HTL is significantly better than that observed with MoO_3 for all different polymer/fullerene blend combinations studied.

It is worth noting that all polymers used in this study are thiophene-based (P3HT, PTB7, and DPPTTT). For PTB7:PC[70]BM-based inverted OPVs, a fast degradation pattern under heating at 85 °C in the dark has previously been observed and has been primarily attributed to morphological changes within the active layer.[38] Furthermore, PTB7 has been reported to be sensitive to several environmental factors,[36,39] whereas DPPTTT has shown a greater stability under light and oxygen[37] but not under thermal conditions.[40] On the other hand, P3HT:PC[70]BM-based inverted OPVs are known to be resistive to several environmental stress factors, and impressive lifetime performances under accelerated and outdoor conditions are demonstrated elsewhere.[41−43]

All above observations indicate that the incorporation of MoO_3 as the HTL at the top electrode of inverted OPVs has a dominant influence on the lifetime performance when subjected to the ISOS D-2 protocol despite the complicated degradation patterns that might also arise because of the variety of active layers. In fact, our study focuses specifically on the electrode configurations in the inverted device structure and the effects of this on the degradation behavior of OPVs. Detailed investigations of the active layer would be beyond the scope of this work. However, the interested reader is referred to the work by Wantz et al.,[44] Rumer and McCulloch,[45] Wang et al.,[43] and Schaffer et al.[46] Our further analyses in the remainder of this study focus on the understanding of the degradation mechanisms of inverted OPVs using our reference and well-optimized P3HT:PC[70]BM as the active layer.

3.2. Investigating the Degradation Mechanisms of P3HT:PC[70]BM/MoO_3-Based Inverted OPVs under the ISOS-D-2 Protocol Using Buffer Layer Engineering. To visualize this fast degradation of P3HT:PC[70]BM-based solar cells, photocurrent images that map the active area of the device and its degradation are shown in Figure 2. This is a powerful technique to understand the spatially resolved photocurrent distribution of complete devices showing a photoelectric effect.[47] A laser is moved across the device through the transparent electrode, giving an indication of defects and therefore possibly diminished device performance. Inverted OPVs using P3HT:PC[70]BM as the active layer and MoO_3 as the HTL were aged, and photocurrent mapping images were extracted at different stages of degradation. The degradation of inverted OPVs with MoO_3 as the HTL occurs very fast, even after 5 h of degradation under heat, and the photocurrent drops dramatically (see Figures 1 and 2).

The photocurrent mapping measurements indicate that for nonencapsulated inverted P3HT:PC[70]BM solar cells incorporating evaporated MoO_3 HTL, the photocurrent generation drops dramatically in just 5 h of exposure. The photocurrent intensity observed is significantly less within the whole device area. Despite the obvious drop near the edges of the devices, which could be attributed to the ingress of air and moisture, the center of the device also shows significantly less photocurrent generation compared with the fresh devices. This is in accordance with Figure 1b, which shows a fast J_{sc} degradation of P3HT:PC[70]BM/MoO_3 within the first few hours of exposure.

To investigate the interfacial interaction of MoO_3 with the P3HT:PC[70]BM active layer, we use buffer layer engineering to isolate the interfaces under study. Inverted OPVs based on P3HT:PC[70]BM with four different configurations of the top electrode—MoO_3/Ag, PEDOT:PSS:ZD/Ag, PEDOT:PSS:ZD/MoO_3/Ag, and MoO_3/PEDOT:PSS:ZD/Ag—were tested under 65 °C. The photovoltaic parameters of these devices are shown in Table 2.

DOI: 10.1021/acsami.7b01183
ACS Appl. Mater. Interfaces 2017, 9, 14136−14144

Table 2. Initial Photovoltaic Parameters and Standard Deviation of Inverted OPVs with Different Hole-Transporting Layers

inverted P3HT:PC[70]BM OPVs using different top electrode configurations	V_{oc} (V)	J_{sc} (mA/cm^2)	FF (%)	PCE (%)
PEDOT:PSS:ZD/Ag	0.582 ± 0.007	9.26 ± 0.38	58.26 ± 2.56	3.16 ± 0.15
PEDOT:PSS:ZD/MoO_3/Ag	0.568 ± 0.014	10.03 ± 0.47	53.65 ± 2.21	3.08 ± 0.17
MoO_3/Ag	0.560 ± 0.009	11.17 ± 0.33	56.41 ± 1.69	3.54 ± 0.15
MoO_3/PEDOT:PSS:ZD/Ag	0.546 ± 0.009	8.52 ± 0.73	57.20 ± 0.81	2.72 ± 0.26

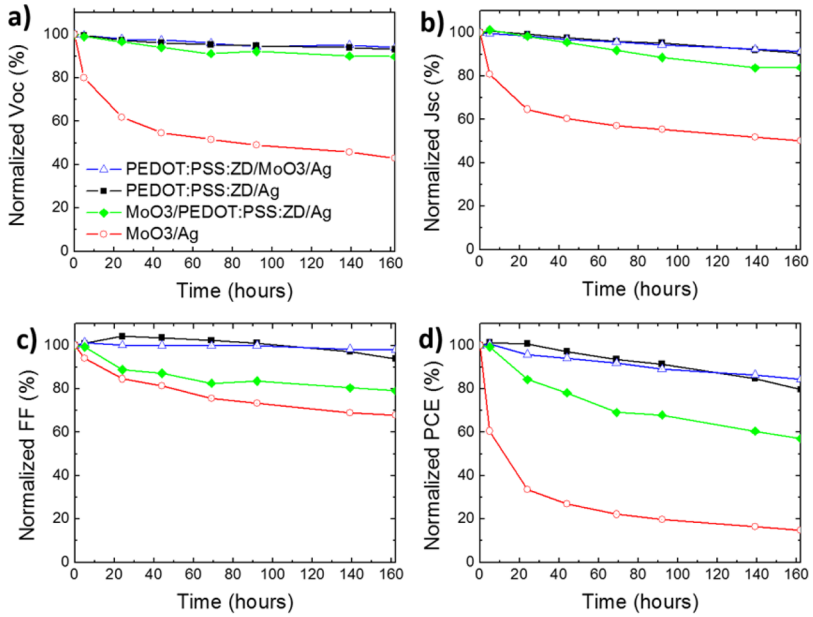

Figure 3. Degradation trends of inverted OPV parameters at 65 °C over time for ITO/ZnO/P3HT:PC[70]BM with different top electrode configurations as a function of (a) normalized V_{oc}, (b) normalized J_{sc}, (c) normalized FF, and (d) normalized PCE.

We observe that the solar cells using the MoO_3/Ag top electrode show the highest initial efficiency of 3.54%. This is followed by very similar device efficiencies of 3.16 and 3.08% obtained using PEDOT:PSS:ZD/Ag and PEDOT:PSS:ZD/MoO_3/Ag, respectively. Finally, a 2.72% PCE is obtained for inverted OPVs with an MoO_3/PEDOT:PSS:ZD/Ag top electrode. Interestingly, these values are comparable to those reported by Wang et al. using a solution-based hybrid electrode consisting of MoO_3 and PEDOT:PSS,[19] indicating an efficient bilayer in our system.

As shown in Figure 3 and in line with the previous observations from Figure 1, inverted OPVs using the MoO_3/Ag top electrode degrade very fast under heat conditions from the initial efficiency of 3.54% compared with inverted OPVs with PEDOT:PSS:ZD as the HTL. As also reported elsewhere,[48] all J/V parameters exponentially drop without allowing precise identification of the failure mechanism. However, by incorporating a PEDOT:PSS:ZD layer between the active layer and MoO_3 as well as between MoO_3 and Ag, the degradation behavior can be influenced.

The inverted OPVs with MoO_3/PEDOT:PSS:ZD/Ag as a top contact present an intermediate PCE decay between devices with MoO_3 and PEDOT:PSS:ZD as HTLs. The majority of the PCE drop in those devices is attributed to FF (Figure 3). Thus, we assume that the influence on FF in devices with MoO_3/Ag top contact is attributed to the interface of MoO_3 and active layer. By inserting the layer of PEDOT:PSS:ZD between MoO_3 and Ag, the suppressed decay of those devices indicates that a direct contact between the MoO_3 and Ag influences device degradation. Furthermore, the decline in the V_{oc} of devices with a direct interface between P3HT:PC[70]BM and MoO_3 (organic/metal oxide interface) is more obvious than that of the devices with P3HT:PC[70]BM and PEDOT:PSS:ZD (organic/organic interface). The latter can again link the failure of the device to the interface of the P3HT:PC[70]BM active layer with MoO_3, as has been reported previously.[48]

On the other hand, inverted OPVs with a PEDOT:PSS:ZD/MoO_3 HTL present lifetime behavior similar to that of inverted OPVs with only PEDOT:PSS:ZD as the HTL. In that case, no obvious degradation is observed when MoO_3 and Ag are in contact. Two possible phenomena could explain this.

The first is that carrier selectivity occurs through PEDOT:PSS:ZD and carrier (i.e., hole) collection occurs through MoO_3/Ag, suggesting that electrons are responsible for the degradation at the MoO_3/Ag interface and that degradation is prevented when the MoO_3/Ag is protected from electrons. This effect was observed by Zhu et al. on inverted hybrid quantum dot/polymer solar cells,[49] in which use of a dual HTL (PEDOT:PSS/MoO_3) led to enhanced electron blocking. This could explain the reduced degradation characteristics observed in our OPVs in which PEDOT:PSS interfaces with the active layer.

The second might be that silver migration and diffusion in the active layer through defects of the MoO_3 layer is prevented by inserting the PEDOT:PSS:ZD layer, as assumed elsewhere.[28,29,48] This effect of atoms diffusing into the active layer has been investigated in several works: The Wantz group has observed a diffusion of silver atoms in MoO_3 and organic layers,[29,48] but interestingly, they did not observe oxygen migration.[50] Additionally, the Österbacka group saw that diffusion of molecules into the active layer material causes

DOI: 10.1021/acsami.7b01183
ACS Appl. Mater. Interfaces 2017, 9, 14136−14144

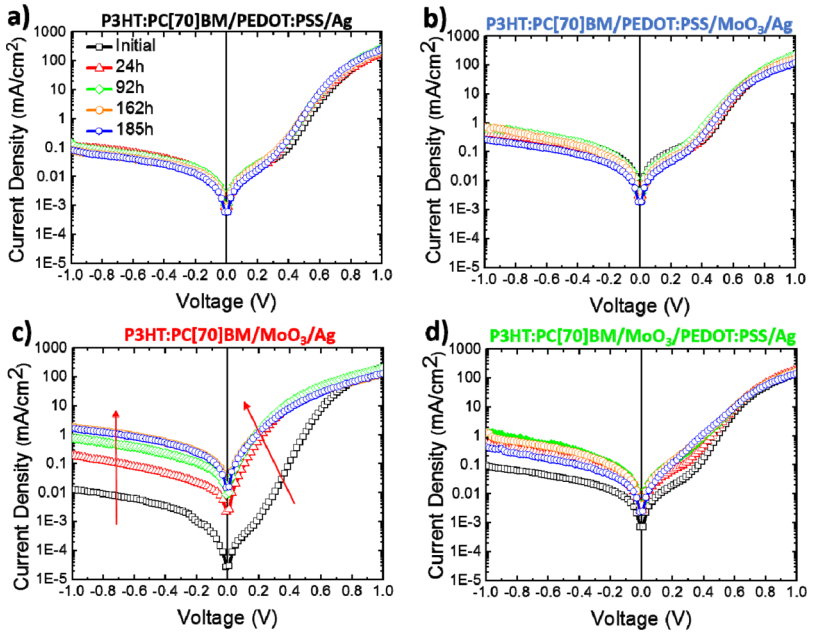

Figure 4. Current density vs voltage characteristics (J/V) in dark over time of exposure under heat conditions for inverted OPVs using different HTLs: (a) PEDOT:PSS:ZD, (b) PEDOT:PSS:ZD/MoO_3, (c) MoO_3, and (d) MoO_3/PEDOT:PSS:ZD.

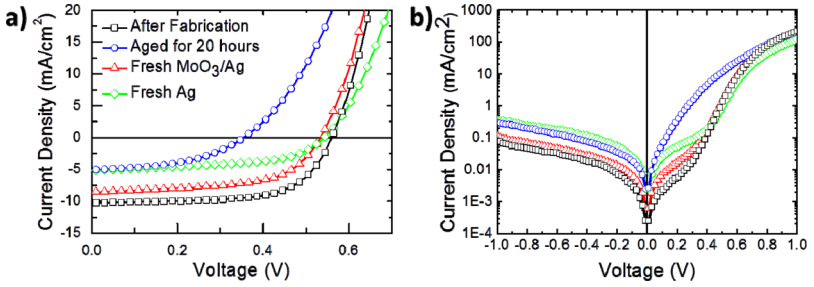

Figure 5. (a) Illuminated and (b) dark J/V characteristics of complete devices with an MoO_3 HTL as produced (black rectangles) and aged for 20 h (blue circles). The incomplete stacks were aged for 20 h at 65 °C and then coated with the required fresh electrode. The stacks were ITO/ZnO/P3HT:PC[70]BM, which was coated with fresh MoO_3/Ag (red triangles), and ITO/ZnO/P3HT:PC[70]BM/MoO_3, which was coated with fresh Ag (green diamonds).

doping effects that are detrimental to the device performance.[51] Our findings for the MoO_3/Ag top contact seem to reflect these behaviors. However, as the detrimental effects have slowed down drastically upon insertion of the PEDOT:PSS:ZD layer in our inverted OPVs, we believe that this is a strong indication that indeed the silver top contact influences these degradation effects also.

Therefore, in our experimental approach, our observations reveal that the interfaces between the active layer and MoO_3 as well as between MoO_3 and Ag majorly contribute to the degradation of the P3HT:PC[70]BM-based inverted OPVs under heat-aging conditions and that electron blocking as well as diffusion of both MoO_3 and Ag species may play a role in this.

To better understand the above observations on the degradation mechanism, the dark J/V characteristics of the different types of OPVs with different buffer layers at the initial and at different stages of degradation were obtained and are shown in Figure 4.

The inverted OPVs containing an MoO_3 HTL as produced and measured in the dark (see Figure 4) have a low leakage current at reverse bias, implying a high shunt resistance (R_p). In addition, at high forward bias, they have high current density and thus low series resistance (R_s) values and therefore their diodelike behavior is better than that of PEDOT:PSS:ZD-containing devices and accordingly they present higher PCE values, as shown in Table 1.

The dark J/V curves of devices with PEDOT:PSS:ZD as the HTL show more stable R_s and R_p values, which are slightly improved over time (Figure 4a). This shows that the organic–organic interface improves over time under heat conditions and that hole transportation is favored at the first stages of degradation. In addition, the performance may be assisted by the formation of a hole-selective thin P3HT layer on the top of the active layer under heating.[9]

Figure 4b shows the dark J/V for devices with PEDOT:PSS:ZD/MoO_3 as the HTL. The R_p of these devices is slightly improved over time, whereas R_s is slightly decreased over time. We assume that the R_p is improved because of the changes in the organic/organic interface. However, we attribute the slight reduction in R_s to the interactions in the double interlayers affecting the carrier transportation in the vertical direction.

Inverted OPVs using MoO_3 as the HTL show slightly reduced R_s over time of exposure. On the other hand, a significant leakage current and ideality factor increase over time,

DOI: 10.1021/acsami.7b01183
ACS Appl. Mater. Interfaces 2017, 9, 14136–14144

implying poor diode properties and MoO_3/active layer interactions (Figure 4c). The increase in R_p of those devices is more intense and more obvious than that of the other inverted OPVs under study, and it occurs even after some hours of degradation. In addition, the R_p and ideality factor issues over time of exposure are also observed when inverted OPVs using MoO_3/PEDOT:PSS:ZD as the HTL are tested (Figure 4d).

The latter reveals the detrimental influence of the P3HT:PC[70]BM/MoO_3 interface in carrier selectivity.[52] This interfacial interaction over time of exposure promotes high leakage current, resulting in poor R_p and ideality factors, which are reflected in FF, as also shown in Figure 3.

3.3. Investigating the Degradation Mechanisms of P3HT:PC[70]BM/MoO_3-Based Inverted OPVs under the ISOS-D-2 Protocol Using Reverse Engineering. Having seen that the inverted OPVs in which MoO_3 directly interfaces with the active layer degrade the fastest, we wanted to investigate whether this interfacial interaction was reversible. We, therefore, fabricated incomplete device structures with ITO/ZnO/P3HT:PC[70]BM and ITO/ZnO/P3HT:PC[70]-BM/MoO_3 stacks. These were aged at 65 °C before the deposition of the subsequent fresh MoO_3/Ag and Ag layers, respectively.

Figure 5 illustrates the illuminated and dark J/V curves for devices with the MoO_3 HTL as-produced and after aging for 20 h at 65 °C. Also, shown are the J/V characteristics for devices with degraded stacks after fresh evaporation of the top contact, enhancing the aspect that the MoO_3/Ag interface also plays a role in this degradation. After reverse engineering,[11] illuminated J/Vs show that the V_{oc} value is recovered when a new MoO_3/Ag is deposited and also only when a new Ag layer is deposited on the ITO/ZnO/P3HT:PC[70]BM/MoO_3 aged stack. This seems to suggest that the MoO_3/Ag interface is responsible for the decay in V_{oc} in devices using MoO_3/Ag top contact.

In addition, the rectification of devices with an active layer/MoO_3 interface changes over time and is getting more symmetrical (Figures 4c,d and 5b). However, in complete devices based on aged ITO/ZnO/P3HT:PC70BM/MoO_3 upon evaporation of a fresh silver electrode or aged ITO/ZnO/P3HT:PC70BM with fresh MoO_3/Ag, the ideality factor of devices with ITO/ZnO/P3HT:PC70BM/MoO_3 and ITO/ZnO/P3HT:PC70BM aged stacks is recovered (see Figure 5) and is similar in shape to the as-produced devices. This is an indicator that in these devices, aging of the MoO_3/Ag interface is responsible for the change in the ideality factor.[48]

However, the fresh evaporation of Ag by itself does not lead to a recovery of J_{sc}. This happens only upon a fresh evaporation of both MoO_3 and Ag on the aged stack of ITO/ZnO/P3HT:PC[70]BM. This could be another indication that the P3HT:PCBM/MoO_3 interface is responsible for the degraded J_{sc} of the device over time of exposure under heat conditions. Overall, with a freshly evaporated MoO_3/Ag electrode, we recover 90% of the efficiency of the as-produced devices, which is a clear indication that the device degradation is not affected by ITO/ZnO/P3HT:PCBM interfaces but almost exclusively by the interfaces of the top electrode P3HT:PCBM/MoO_3/Ag, as shown in Figure 5. It should be noted that in principle, we expected to reach the same efficiency with the as-produced devices. However, we assume that the exposure to moisture in combination with the heat causes faster degradation and interface modification than the uncapped devices, thereby preventing full recovery by reverse engineering the top contact.

4. CONCLUSIONS

We monitored the lifetime performance of P3HT:PC[70]BM, PTB7:PC[70]BM, and DPPTTT:PC[70]BM inverted OPVs using thermally evaporated MoO_3 as the HTL under heat conditions according to the ISOS-D-2 protocol (T = 65 °C, dark, and constant ambient RH of ∼40%). Inverted P3HT:PC[70]BM OPVs using thermally evaporated MoO_3 as the HTL presented the most dramatic decay in all OPV parameters under 65 °C even after a few hours of exposure. A series of experiments were performed using photocurrent mapping and different device architectures to isolate the interfaces and reveal the failure mechanisms of P3HT:PC[70]-BM devices under accelerated-heat conditions.

Upon incorporation of the two compared HTLs (evaporated MoO_3 and solution-processed PEDOT:PSS:ZD) in different configurations in inverted OPVs with the P3HT:PC[70]BM active layer, we observed that the P3HT:PC[70]BM/MoO_3 interface is the most sensitive part of this degradation triggered at 65 °C. This is primarily shown by the reduction in FF and slower degradation of inverted OPVs with the MoO_3/PEDOT:PSS:ZD double interlayer, which isolates the MoO_3 from the Ag. This was in agreement with the dark J/Vs of inverted OPVs, which show that the ideality factor of OPVs with the P3HT:PC[70]BM/MoO_3 interface is affected, thereby further revealing the detrimental influence of this interface. After an alternative reverse engineering method, we showed that the V_{oc} and the ideality factor of such devices are recovered when fresh Ag is deposited on the top of the aged ITO/ZnO/P3HT:PC[70]BM/MoO_3 stacks. This showed that the Ag electrode influences the stability of inverted OPVs with MoO_3 as the HTL under heat conditions and was confirmed by the suppressed decay of inverted OPVs using MoO_3/PEDOT:PSS:ZD as the HTL.

To conclude, in the case of inverted P3HT:PC[70]BM OPVs with MoO_3/Ag top contact, which were extensively studied in this paper using a series of measurements and device/reverse engineering methods, the results presented indicate that the heat degradation of the inverted OPVs is not affected by the ITO/ZnO/P3HT:PCBM interfaces but almost exclusively by the interfaces of the top electrode P3HT:PCBM/MoO_3/Ag. Although the interface between MoO_3 and Ag contributes to degradation, the interface between the P3HT:PC[70]BM active layer and MoO_3 is the main origin of failure of inverted OPVs under intense heat conditions, a trend that was observed for the three thiophene-based materials used in this study of inverted OPVs. The PEDOT:PSS:ZD HTL resulted in a more stable inverted OPV performance compared with MoO_3 HTL under the ISOS-D-2 heat protocol, a fact which should be taken into account when reporting high-efficiency devices using MoO_3 as the HTL.

AUTHOR INFORMATION

Corresponding Author

*E-mail: stelios.choulis@cut.ac.cy.

ORCID

James R. Durrant: 0000-0001-8353-7345
Iain McCulloch: 0000-0002-6340-7217
Stelios A. Choulis: 0000-0002-7899-6296

Author Contributions

The manuscript was written through contributions of all authors. All authors have given approval to the final version of the manuscript.

DOI: 10.1021/acsami.7b01183
ACS Appl. Mater. Interfaces 2017, 9, 14136−14144

Notes

The authors declare no competing financial interest.

■ ACKNOWLEDGMENTS

Funding from the European Research Council (H2020-ERC-2014-GoG project number 647311) is gratefully acknowledged.

■ REFERENCES

(1) Hösel, M.; Søndergaard, R. R.; Angmo, D.; Krebs, F. C. Comparison of Fast Roll-to-Roll Flexographic, Inkjet, Flatbed, and Rotary Screen Printing of Metal Back Electrodes for Polymer Solar Cells. *Adv. Eng. Mater.* **2013**, *15*, 995−1001.

(2) Krebs, F. C. Fabrication and Processing of Polymer Solar Cells: A Review of Printing and Coating Techniques. *Sol. Energy Mater. Sol. Cells* **2009**, *93*, 394−412.

(3) Green, M. A.; Emery, K.; Hishikawa, Y.; Warta, W.; Dunlop, E. D. Solar Cell Efficiency Tables (Version 45). *Prog. Photovoltaics* **2015**, *23*, 1−9.

(4) Steim, R.; Choulis, S. A.; Schilinsky, P.; Brabec, C. J. Interface Modification for Highly Efficient Organic Photovoltaics. *Appl. Phys. Lett.* **2008**, *92*, 093303.

(5) Waldauf, C.; Morana, M.; Denk, P.; Schilinsky, P.; Coakley, K.; Choulis, S. A.; Brabec, C. J. Highly Efficient Inverted Organic Photovoltaics Using Solution Based Titanium Oxide as Electron Selective Contact. *Appl. Phys. Lett.* **2006**, *89*, 233517.

(6) Lira-Cantu, M.; Tanenbaum, D. M.; Norrman, K.; Voroshazi, E.; Hermenau, M.; Lloyd, M. T.; Teran-Escobar, G.; Galagan, Y.; Zimmermann, B.; Hösel, M.; Dam, H. F.; Jørgensen, M.; Gevorgyan, S.; Lutsen, L.; Vanderzande, D.; Hoppe, H.; Rösch, R.; Würfel, U.; Andriessen, R.; Rivaton, A.; Uzunoğlu, G. Y.; Germack, D.; Andreasen, B.; Madsen, M. V.; Bundgaard, E.; Krebs, F. C. Combined Characterization Techniques to Understand the Stability of a Variety of Organic Photovoltaic Devices: The ISOS-3 Inter-Laboratory Collaboration. In *Proc. SPIE 8472, Reliability of Photovoltaic Cells, Modules, Components, and Systems V*; 2012; pp 847203−847206.

(7) Adams, J.; Salvador, M.; Lucera, L.; Langner, S.; Spyropoulos, G. D.; Fecher, F. W.; Voigt, M. M.; Dowland, S. A.; Osvet, A.; Egelhaaf, H.-J.; Brabec, C. J. Water Ingress in Encapsulated Inverted Organic Solar Cells: Correlating Infrared Imaging and Photovoltaic Performance. *Adv. Energy Mater.* **2015**, *5*, 1501065.

(8) Glen, T. S.; Scarratt, N. W.; Yi, H.; Iraqi, A.; Wang, T.; Kingsley, J.; Buckley, A. R.; Lidzey, D. G.; Donald, A. M. Dependence on Material Choice of Degradation of Organic Solar Cells Following Exposure to Humid Air. *J. Polym. Sci., Part B: Polym. Phys.* **2015**, *54*, 216−224.

(9) Sachs-Quintana, I. T.; Heumüller, T.; Mateker, W. R.; Orozco, D. E.; Cheacharoen, R.; Sweetnam, S.; Brabec, C. J.; McGehee, M. D. Electron Barrier Formation at the Organic-Back Contact Interface is the First Step in Thermal Degradation of Polymer Solar Cells. *Adv. Funct. Mater.* **2014**, *24*, 3978−3985.

(10) Kawano, K.; Pacios, R.; Poplavskyy, D.; Nelson, J.; Bradley, D. D. C.; Durrant, J. R. Degradation of Organic Solar Cells Due to Air Exposure. *Sol. Energy Mater. Sol. Cells* **2006**, *90*, 3520−3530.

(11) Drakonakis, V. M.; Savva, A.; Kokonou, M.; Choulis, S. A. Investigating Electrodes Degradation in Organic Photovoltaics through Reverse Engineering under Accelerated Humidity Lifetime Conditions. *Sol. Energy Mater. Sol. Cells* **2014**, *130*, 544−550.

(12) Lloyd, M. T.; Peters, C. H.; Garcia, A.; Kauvar, I. V.; Berry, J. J.; Reese, M. O.; McGehee, M. D.; Ginley, D. S.; Olson, D. C. Influence of the Hole-Transport Layer on the Initial Behavior and Lifetime of Inverted Organic Photovoltaics. *Sol. Energy Mater. Sol. Cells* **2011**, *95*, 1382−1388.

(13) Lloyd, M. T.; Olson, D. C.; Lu, P.; Fang, E.; Moore, D. L.; White, M. S.; Reese, M. O.; Ginley, D. S.; Hsu, J. W. P. Impact of Contact Evolution on the Shelf Life of Organic Solar Cells. *J. Mater. Chem.* **2009**, *19*, 7638−7642.

(14) Savva, A.; Georgiou, E.; Papazoglou, G.; Chrusou, A. Z.; Kapnisis, K.; Choulis, S. A. Photovoltaic Analysis of the Effects of PEDOT:PSS-Additives Hole Selective Contacts on the Efficiency and Lifetime Performance of Inverted Organic Solar Cells. *Sol. Energy Mater. Sol. Cells* **2015**, *132*, 507−514.

(15) Norrman, K.; Madsen, M. V.; Gevorgyan, S. A.; Krebs, F. C. Degradation Patterns in Water and Oxygen of an Inverted Polymer Solar Cell. *J. Am. Chem. Soc.* **2010**, *132*, 16883−16892.

(16) Zilberberg, K.; Gharbi, H.; Behrendt, A.; Trost, S.; Riedl, T. Low-Temperature, Solution-Processed MoO_x for Efficient and Stable Organic Solar Cells. *ACS Appl. Mater. Interfaces* **2012**, *4*, 1164−1168.

(17) Qiu, W.; Müller, R.; Voroshazi, E.; Conings, B.; Carleer, R.; Boyen, H.-G.; Turbiez, M.; Froyen, L.; Heremans, P.; Hadipour, A. Nafion-Modified MoO_x as Effective Room-Temperature Hole Injection Layer for Stable, High-Performance Inverted Organic Solar Cells. *ACS Appl. Mater. Interfaces* **2015**, *7*, 3581−3589.

(18) Kim, J.-H.; Park, E.-K.; Kim, J.-H.; Cho, H. J.; Lee, D.-H.; Kim, Y.-S. Improving Charge Transport of P3HT:PCBM Organic Solar Cell Using MoO_3 Nanoparticles as an Interfacial Buffer Layer. *Electron. Mater. Lett.* **2016**, *12*, 383−387.

(19) Wang, Y.; Luo, Q.; Wu, N.; Wang, Q.; Zhu, H.; Chen, L.; Li, Y.-Q.; Luo, L.; Ma, C.-Q. Solution-Processed MoO_3:PEDOT:PSS Hybrid Hole Transporting Layer for Inverted Polymer Solar Cells. *ACS Appl. Mater. Interfaces* **2015**, *7*, 7170−7179.

(20) Hammond, S. R.; Meyer, J.; Widjonarko, N. E.; Ndione, P. F.; Sigdel, A. K.; Garcia, A.; Miedaner, A.; Lloyd, M. T.; Kahn, A.; Ginley, D. S.; Berry, J. J.; Olson, D. C. Low-Temperature, Solution-Processed Molybdenum Oxide Hole-Collection Layer for Organic Photovoltaics. *J. Mater. Chem.* **2012**, *22*, 3249−3254.

(21) Park, S.; Jeong, J.; Hyun, G.; Kim, M.; Lee, H.; Yi, Y. The Origin of High PCE in PTB7 Based Photovoltaics: Proper Charge Neutrality Level and Free Energy of Charge Separation at PTB7/PC71BM Interface. *Sci. Rep.* **2016**, *6*, 35262.

(22) Weerasinghe, H. C.; Watkins, S. E.; Duffy, N.; Jones, D. J.; Scully, A. D. Influence of Moisture Out-Gassing from Encapsulant Materials on the Lifetime of Organic Solar Cells. *Sol. Energy Mater. Sol. Cells* **2015**, *132*, 485−491.

(23) Irfan; Ding, H.; Gao, Y.; Small, C.; Kim, D. Y.; Subbiah, J.; So, F. Energy Level Evolution of Air and Oxygen Exposed Molybdenum Trioxide Films. *Appl. Phys. Lett.* **2010**, *96*, 243307.

(24) Griffin, J.; Watters, D. C.; Yi, H.; Iraqi, A.; Lidzey, D.; Buckley, A. R. The Influence of MoO_x Anode Stoicheometry on the Performance of Bulk Heterojunction Polymer Solar Cells. *Adv. Energy Mater.* **2013**, *3*, 903−908.

(25) Voroshazi, E.; Cardinaletti, I.; Uytterhoeven, G.; Li, S.; Empl, M.; Aernouts, T.; Rand, B. P. Role of Electron- and Hole-Collecting Buffer Layers on the Stability of Inverted Polymer:Fullerene Photovoltaic Devices. *IEEE J. Photovolt.* **2014**, *4*, 265−270.

(26) Zhang, Z.; Xiao, Y.; Wei, H.-X.; Ma, G.-F.; Duhm, S.; Li, Y.-Q.; Tang, J.-X. Impact of Oxygen Vacancy on Energy-Level Alignment at MoO_X/Organic Interfaces. *Appl. Phys. Express* **2013**, *6*, 095701.

(27) Voroshazi, E.; Uytterhoeven, G.; Cnops, K.; Conard, T.; Favia, P.; Bender, H.; Muller, R.; Cheyns, D. Root-Cause Failure Analysis of Photocurrent Loss in Polythiophene:Fullerene-Based Inverted Solar Cells. *ACS Appl. Mater. Interfaces* **2015**, *7*, 618−623.

(28) Rösch, R.; Tanenbaum, D. M.; Jørgensen, M.; Seeland, M.; Bärenklau, M.; Hermenau, M.; Voroshazi, E.; Lloyd, M. T.; Galagan, Y.; Zimmermann, B.; Würfel, U.; Hösel, M.; Dam, H. F.; Gevorgyan, S. A.; Kudret, S.; Maes, W.; Lutsen, L.; Vanderzande, D.; Andriessen, R.; Teran-Escobar, G.; Lira-Cantu, M.; Rivaton, A.; Uzunoğlu, G. Y.; Germack, D.; Andreasen, B.; Madsen, M. V.; Norrman, K.; Hoppe, H.; Krebs, F. C. Investigation of the Degradation Mechanisms of a Variety of Organic Photovoltaic Devices by Combination of Imaging Techniques—The ISOS-3 Inter-Laboratory Collaboration. *Energy Environ. Sci.* **2012**, *5*, 6521.

(29) Greenbank, W.; Rolston, N.; Destouesse, E.; Wantz, G.; Hirsch, L.; Dauskardt, R.; Chambon, S. Improved Mechanical Adhesion and Electronic Stability of Organic Solar Cells with Thermal Ageing: The Role of Diffusion at the Hole Extraction Interface. *J. Mater. Chem. A* **2017**, *5*, 2911−2919.

DOI: 10.1021/acsami.7b01183
ACS Appl. Mater. Interfaces 2017, 9, 14136−14144

(30) Savva, A.; Choulis, S. A. Cesium-Doped Zinc Oxide as Electron Selective Contact in Inverted Organic Photovoltaics. *Appl. Phys. Lett.* **2013**, *102*, 233301.
(31) Savva, A.; Neophytou, M.; Koutsides, C.; Kalli, K.; Choulis, S. A. Synergistic Effects of Buffer Layer Processing Additives for Enhanced Hole Carrier Selectivity in Inverted Organic Photovoltaics. *Org. Electron.* **2013**, *14*, 3123−3130.
(32) Reese, M. O.; Gevorgyan, S. A.; Jørgensen, M.; Bundgaard, E.; Kurtz, S. R.; Ginley, D. S.; Olson, D. C.; Lloyd, M. T.; Morvillo, P.; Katz, E. A.; Elschner, A.; Haillant, O.; Currier, T. R.; Shrotriya, V.; Hermenau, M.; Riede, M.; Kirov, K. R.; Trimmel, G.; Rath, T.; Inganäs, O.; Zhang, F.; Andersson, M.; Tvingstedt, K.; Lira-Cantu, M.; Laird, D.; McGuiness, C.; Gowrisanker, S.; Pannone, M.; Xiao, M.; Hauch, J.; Steim, R.; DeLongchamp, D. M.; Rösch, R.; Hoppe, H.; Espinosa, N.; Urbina, A.; Yaman-Uzunoglu, G.; Bonekamp, J.-B.; van Breemen, A. J. J. M.; Girotto, C.; Voroshazi, E.; Krebs, F. C. Consensus Stability Testing Protocols for Organic Photovoltaic Materials and Devices. *Sol. Energy Mater. Sol. Cells* **2011**, *95*, 1253−1267.
(33) Dang, M. T.; Hirsch, L.; Wantz, G. P3HT:PCBM, Best Seller in Polymer Photovoltaic Research. *Adv. Mater.* **2011**, *23*, 3597−3602.
(34) He, Z.; Zhong, C.; Su, S.; Xu, M.; Wu, H.; Cao, Y. Enhanced Power-Conversion Efficiency in Polymer Solar Cells Using an Inverted Device Structure. *Nat. Photonics* **2012**, *6*, 593−597.
(35) Lu, L.; Yu, L. Understanding Low Bandgap Polymer PTB7 and Optimizing Polymer Solar Cells Based on It. *Adv. Mater.* **2014**, *26*, 4413−4430.
(36) Wong, H. C.; Li, Z.; Tan, C. H.; Zhong, H.; Huang, Z.; Bronstein, H.; McCulloch, I.; Cabral, J. T.; Durrant, J. R. Morphological Stability and Performance of Polymer−Fullerene Solar Cells under Thermal Stress: The Impact of Photoinduced PC60BM Oligomerization. *ACS Nano* **2014**, *8*, 1297−1308.
(37) Soon, Y. W.; Cho, H.; Low, J.; Bronstein, H.; McCulloch, I.; Durrant, J. R. Correlating Triplet Yield, Singlet Oxygen Generation and Photochemical Stability in Polymer/Fullerene Blend Films. *Chem. Commun.* **2013**, *49*, 1291.
(38) Tessarolo, M.; Guerrero, A.; Gedefaw, D.; Bolognesi, M.; Prosa, M.; Xu, X.; Mansour, M.; Wang, E.; Seri, M.; Andersson, M. R.; Muccini, M.; Garcia-Belmonte, G. Predicting Thermal Stability of Organic Solar Cells through an Easy and Fast Capacitance Measurement. *Sol. Energy Mater. Sol. Cells* **2015**, *141*, 240−247.
(39) Razzell-Hollis, J.; Wade, J.; Tsoi, W. C.; Soon, Y.; Durrant, J.; Kim, J.-S. Photochemical Stability of High Efficiency PTB7:PC70BM Solar Cell Blends. *J. Mater. Chem. A* **2014**, *2*, 20189−20195.
(40) Huang, Z.; Fregoso, E. C.; Dimitrov, S.; Tuladhar, P. S.; Soon, Y. W.; Bronstein, H.; Meager, I.; Zhang, W.; McCulloch, I.; Durrant, J. R. Optimisation of Diketopyrrolopyrrole:Fullerene Solar Cell Performance through Control of Polymer Molecular Weight and Thermal Annealing. *J. Mater. Chem. A* **2014**, *2*, 19282−19289.
(41) Hauch, J. A.; Schilinsky, P.; Choulis, S. A.; Childers, R.; Biele, M.; Brabec, C. J. Flexible Organic P3HT:PCBM Bulk-Heterojunction Modules with More Than 1 Year Outdoor Lifetime. *Sol. Energy Mater. Sol. Cells* **2008**, *92*, 727−731.
(42) Sapkota, S. B.; Spies, A.; Zimmermann, B.; Dürr, I.; Würfel, U. Promising Long-Term Stability of Encapsulated Ito-Free Bulk-Heterojunction Organic Solar Cells under Different Aging Conditions. *Sol. Energy Mater. Sol. Cells* **2014**, *130*, 144−150.
(43) Wang, W.; Schaffer, C. J.; Song, L.; Körstgens, V.; Pröller, S.; Indari, E. D.; Wang, T.; Abdelsamie, A.; Bernstorff, S.; Müller-Buschbaum, P. In Operando Morphology Investigation of Inverted Bulk Heterojunction Organic Solar Cells by GalaxsISAXS. *J. Mater. Chem. A* **2015**, *3*, 8324−8331.
(44) Wantz, G.; Derue, L.; Dautel, O.; Rivaton, A.; Hudhomme, P.; Dagron-Lartigau, C. Stabilizing Polymer-Based Bulk Heterojunction Solar Cells via Crosslinking. *Polym. Int.* **2014**, *63*, 1346−1361.
(45) Rumer, J. W.; McCulloch, I. Organic Photovoltaics: Crosslinking for Optimal Morphology and Stability. *Mater. Today* **2015**, *18*, 425−435.
(46) Schaffer, C. J.; Palumbiny, C. M.; Niedermeier, M. A.; Jendrzejewski, C.; Santoro, G.; Roth, S. V.; Müller-Buschbaum, P. A Direct Evidence of Morphological Degradation on a Nanometer Scale in Polymer Solar Cells. *Adv. Mater.* **2013**, *25*, 6760−6764.
(47) Bonekamp, J.-B.; Moulé, A. J.; Meerholz, K. Detailed Study of the Decay Mechanism in Polymeric Oleds. In *Organic Light-Emitting Materials and Devices IX*; SPIE, 2005; Vol. *5937*, p 593713.
(48) Greenbank, W. A.; Hirsch, L.; Wantz, G.; Chambon, S. Interfacial Thermal Degradation in Inverted Organic Solar Cells. *Appl. Phys. Lett.* **2015**, *107*, 263301.
(49) Zhu, L.; Richardson, B. J.; Yu, Q. Inverted Hybrid CdSe−Polymer Solar Cells Adopting PEDOT:PSS/MoO_3 as Dual Hole Transport Layers. *Phys. Chem. Chem. Phys.* **2016**, *18*, 3463−3471.
(50) Chambon, S.; Derue, L.; Lahaye, M.; Pavageau, B.; Hirsch, L.; Wantz, G. MoO_3 Thickness, Thermal Annealing and Solvent Annealing Effects on Inverted and Direct Polymer Photovoltaic Solar Cells. *Materials* **2012**, *5*, 2521−2536.
(51) Nyman, M.; Dahlström, S.; Sandberg, O. J.; Österbacka, R. Unintentional Bulk Doping of Polymer-Fullerene Blends from a Thin Interfacial Layer of MoO_3. *Adv. Energy Mater.* **2016**, *6*, 1600670.
(52) Lee, K. E.; Liu, L.; Kelly, T. L. Effect of Molybdenum Oxide Electronic Structure on Organic Photovoltaic Device Performance: An X-ray Absorption Spectroscopy Study. *J. Phys. Chem. C* **2014**, *118*, 27735−27741.

DOI: 10.1021/acsami.7b01183
ACS Appl. Mater. Interfaces 2017, 9, 14136−14144